Hybrid Thermochemical Cycle for Cold and Electricity Cogeneration: Experimental Analysis of the Process Behavior and Expander-Reactor Coupling

Hasan Ghazale, Nathalie Mazet, Pierre Neveu, Maxime Perier-Muzet

PROCEEDINGS OF ECOS 2023 - THE 36TH INTERNATIONAL CONFERENCE ON
EFFICIENCY, **C**OST, **O**PTIMIZATION, **S**IMULATION AND ENVIRONMENTAL IMPACT OF ENERGY SYSTEMS
25-30 JUNE, 2023, LAS PALMAS DE GRAN CANARIA, SPAIN

Hybrid thermochemical cycle for cold and electricity cogeneration: experimental analysis of the process behavior and expander-reactor coupling

Hasan Ghazale[a], Nathalie Mazet[b], Pierre Neveu[c] and Maxime Perier-Muzet[d]

[a] CNRS-PROMES. Laboratoire PROcédés, Matériaux et Energie Solaire, Perpignan, France, Hasan.ghazale@promes.cnrs.fr, CA

[b] CNRS-PROMES. Laboratoire PROcédés, Matériaux et Energie Solaire, Perpignan, France, mazet@univ-perp.fr

[c] CNRS-PROMES. Laboratoire PROcédés, Matériaux et Energie Solaire, Perpignan, France, neveu@univ-perp.fr

[d] CNRS-PROMES. Laboratoire PROcédés, Matériaux et Energie Solaire, Perpignan, France, maxime.perier-muzet@univ-perp.fr

Abstract :

The valorisation of waste heat to respond to the increase demand on electricity and cooling is an important energetic challenge. For this purpose, an original hybrid thermochemical cycle is proposed: this sorption cycle is based on reversible endothermic/exothermic solid-gas reactions, and its originality lies in the integration of an expander on the gas line to provide mechanical work. This tri-thermal discontinuous cycle is able to recover medium grade waste heat (between 150 and 250 °C) to valorise it in a second step by providing cold production at its endothermic component and mechanical work - thanks to the expander - on the gas flow. Moreover, its two step operation leads to a storage functionality. While a previous study holds the thermodynamic stationary analysis of this cycle (Godefroy et al., ECOS 2019), this paper presents the experimental study part. A prototype of the hybrid thermochemical cycle, with $MnCl_2(6/2)NH_3$ (solid-gas reactants) and 1 kWe scroll expander, is developed at the laboratory. First experimentations on the prototype proved on a side the hybrid thermochemical concept by the simultaneous cold and mechanical productions during the whole reaction of the production phase, and on the other side they showed experimentally the mass coupling behaviour between the reactor and the expander in several operating conditions.

Keywords: Hybrid thermochemical cycle; Heat waste recovery; Cold and work productions; Experimental prototype.

1. Introduction

1.1. Background and state of the art

Sustainable development that meets the needs of the present without promising the ability of future generations to meet their own needs has been announced in 1987 by the World Commission on Environment and Development [1]. The acceptance and reliability of solar energy and waste heat come in the same context while considering such sources of energies as emerging sources since they are always free, endless and convertible [2]. Waste heat is highly discharged at the industrial sectors in a wide temperature range and thus participating in the increase of greenhouse gas emissions and more resource consumptions while left useless. As a step in responding to this issue, the United Nations Environment Program proposed industrial ecology, which involves studying the relationships and interactions within and between industrial systems and natural ecological systems from a systems-oriented perspective [3]. On this way also, conversion technologies and cycles based on the wide temperature ranges of the released heat at the industries were developed and set under study. Absorption chillers, adsorption beds, thermochemical reaction processes were exploited in this theme showing their adaptability in such temperature ranges (even low and medium) as chemical heat pumps for temperature upgrading. Besides, steam and organic Rankine cycles were investigated also but for power generation purposes.

As industrial waste heat has an intermittent regime, processes like thermochemical attract attention due to the storage functionality they offer.

Among such solid-gas thermochemical processes, ammoniated ones have a large diversity due to the variety of solid salts that can react with ammonia – especially the chlorides [4]. Being integrated with an expander, hybrid thermochemical cycles were defined to valorise mass and heat transfers in thermal and electrical productions. In [5], a novel "resorption" (two-salt bed reactors) cycle for cogeneration of electricity and refrigeration was proposed featuring a turbine between the high and low temperature salt reactors. Numerical analysis of a single sorption cycle was performed and investigated in [6]. Results showed a limited performance of the cycle resulted from the mutual constraint between the expansion device and the sorption unit with a detectable mismatch between them. Experimentally, by having $CaCl_2$ and activated carbon as the sorbent unit and a scroll expander, the challenges were confirmed by [7] where only unstable and weak work production was achieved during the experiment. A second experiment was performed in [8], the resorption pairs was $MnCl_2$ & $CaCl_2$, and similarly unstable work production was noticed during the short process. Such challenges haven't stopped the research, so that in [9] the use of phase change material in a heat storage system combined with a thermochemical hybrid process was addressed. In [10], more than one hundred reactive ammoniated salts were scanned and analysed in a hybrid thermochemical cycle that can recover heat below than 250 °C. Moreover, it was shown that these hybrid thermochemical cycles offer inherent cogeneration and storage capabilities, as demonstrated in [11] and [12], representing an added value compared to more traditional solutions. This paper continues the research in hybrid thermochemical processes, where an experimental prototype is developed at CNRS-PROMES permitting to validate the hybrid concept by continuous cold and mechanical productions during the production phase, and to analyse the cycle's behaviour and the coupling between the expander and the reactor in different operating conditions.

1.2. The proposed cycle

Several architectures were defined for the hybrid thermochemical cycle [13] depending on the preferred energy production: cold or mechanical. In this study, the simultaneous mode is chosen for the developed prototype: it allows a cogeneration of cold and mechanical energy as presented on the Clausius Clapeyron diagram, Figure. **1**. Figure. **2** shows the main components of the prototype: thermochemical reactor, condenser, evaporator, volumetric expander and fluid tank. The decomposition reaction of the solid-gas reactant is the charging phase where heat Q_h is supplied to the reactor at T_{hot} and the gas desorbs toward the condenser to be condensed and stored at ambient conditions T_{amb}. During the discharging phase (synthesis reaction), cold is produced by the evaporation of the condensed liquid at T_{cold} at the evaporator. This vapor flow produces then mechanical work at the expander, and after it is then involved in the synthesis reaction occurring at ambient conditions (or at a medium temperature). $MnCl_2$, (6/2) NH_3 is the chosen reactive ammoniated salt, based on its interesting thermodynamic properties and stability as shown in the analysis of [10]. The thermochemical reaction that takes place is:

$$MnCl_2.6NH_3 + \Delta h_r \rightleftarrows MnCl_2.2NH_3 + 4NH_3 \qquad (1)$$

The diagram, Figure. **1**, presents the NH3(L/G) and MnCl2(6/2) NH3 equilibrium lines for ammonia and the reaction respectively, based on the Clausius Clapeyron equilibrium equation:

$$\ln\left(\frac{p}{p_0}\right) = -\frac{\Delta h_r}{RT_r} + \frac{\Delta s_r}{R} \qquad (2)$$

where, p is the equilibrium pressure, p_0 is the reference pressure (1 bar), R is the ideal gas constant, Δh_r and Δs_r are respectively the enthalpy and the entropy of the solid gas reaction or the phase change of ammonia and T_r is the reactant temperature.

A scroll expander is integrated within the thermochemical cycle between the evaporator and the reactor. The control parameter of the bench are the temperatures and flowrates of all heat transfer fluids (HTF), with the electrical resistance at the generator bounds. Temperatures are measured with PT100 probes for the inlet/outlet of HTFs, and by numerous thermocouples inside the reactor (in the reactive solid (12 thermocouples), at the reactor wall (8 thermocouples) and in the HTF (8 thermocouples)). The pressure of the main components (evaporator, expander, condenser and reactor) and the level of liquid ammonia in the tank (linked to the reaction advancement) are also monitored.

In what follows, experimental analysis of cycle is done showing the proved concept of the hybrid thermochemical cycle and the coupling between its components.

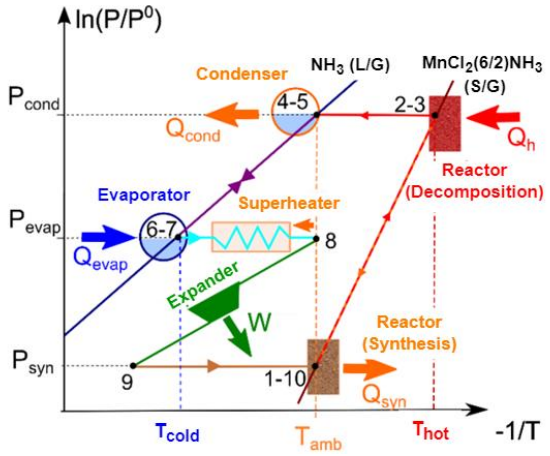

Figure. 1. Simultaneous hybrid thermochemical cycle described on the Clausius Clapeyron diagram.

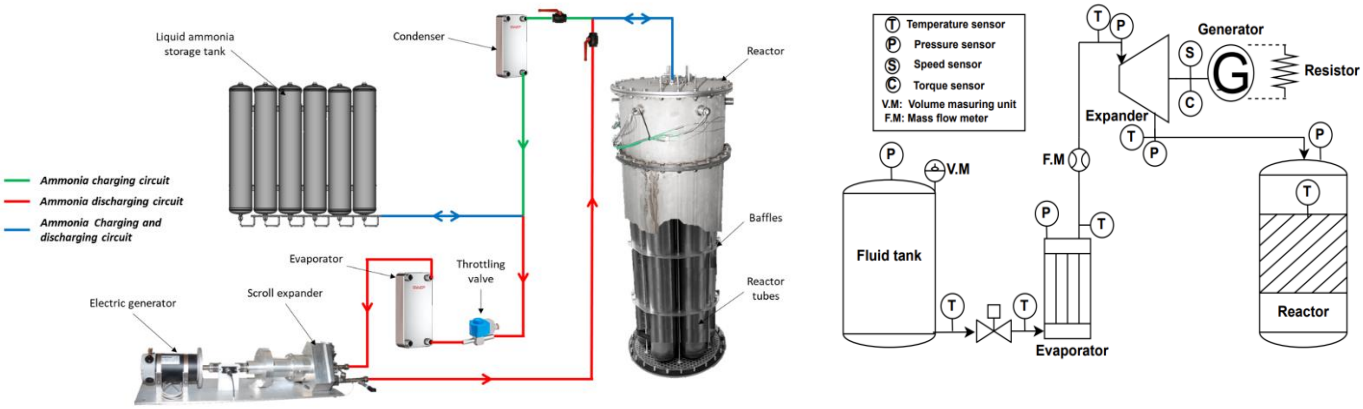

Figure. 2. Left: Schematic description of the developed prototype: reactor with 29 Kg of $MnCl_2$ & 23 kg of NH_3, 1 kWe scroll expander (bought from Air squared), condenser, evaporator, throttling valve & fluid tanks. Right: Process flow diagram: cold and mechanical productions phase.

2. Numerical analysis of the expander/reactor coupling

To analyse from a theoretical point of view the coupling between the expander and the reactor, a simplified modelling of these components has been developed.

The main hypotheses of this analysis are as follows:

- Steady state operation;
- The working fluid is considered as an ideal gas with constant heat mass capacity;
- Uniform pressure, temperature and composition are considered in each component;
- Heat losses and pressure drops are neglected;
- Variation of kinetic and potential energy are neglected.

By applying the first law on the expander, the expansion power of the working fluid can be expressed as:

$$\dot{W}_{NH_3} = \dot{m}_{swept} \cdot \Delta h_{swept} \qquad (3)$$

Having the mass flow rate expression as:

$$\dot{m}_{NH_3} = \dot{m}_{swept} + \dot{m}_{leak} = \frac{p_{adm}.M_{NH_3}}{R \cdot T_{adm}} \left(\dot{V}_{swept} + \dot{V}_{leak} \right) = \frac{p_{adm}.M_{NH_3}}{R \cdot T_{adm}} \left(V_{swept} \cdot \omega + K_{leak} \cdot \sqrt{p_{adm} - p_{exh}} \right) \quad (4)$$

With p_{adm} and T_{adm} are the pressure and temperature at the expander admission, V_{swept} is the swept volume and ω the rotational speed, K_{leak} is the coefficient of internal leakage of the expander and p_{exh} is the pressure at the expander exhaust.

The enthalpy variation is expressed, considering a constant isentropic efficiency:

$$\eta_{is} = \frac{\Delta h_{swept}}{\Delta h_{is}} \rightarrow \Delta h_{swept} = \eta_{is} \cdot \Delta h_{is} \qquad (5)$$

With the ideal gas assumption and a constant Cp, the swept enthalpy variation is as:

$$\Delta h_{swept} = \eta_{is} \cdot Cp_{NH3} \cdot T_{adm} \cdot \left(\left(p_{adm} / p_{exh} \right)^{\frac{1-\gamma}{\gamma}} - 1 \right) \qquad (6)$$

The exhaust pressure can be expressed, thanks to the kinetic law of the reactor, as:

$$\dot{m}_{NH3} = M_{NH_3} \cdot n_{sal} \cdot \nu_r \cdot \tilde{k}_{cin} \cdot \frac{p_{exh} - p_{eq}(T_r)}{p_{exh}} \text{ and thus: } p_{exh} = \frac{p_{eq}(T_r)}{\left(1 - \frac{\dot{m}_{NH3}}{M_{NH_3} \cdot n_{salt} \cdot \nu_r \cdot \bar{k}_{cin}} \right)} \qquad (7)$$

Where:

- $n_{salt,}$ $\nu_{r,}$ and $\bar{k}_{cin}$ are the number of mole of the reactive salt in the reactor, the stoichiometric coefficient of the reaction (eq. 1), and the average kinetic coefficient of the reaction;

- the solid/gas equilibrium pressure is calculated, thanks to the Clausius-Clapeyron equation (eq. 2), as a function of the reactant temperature (T_r).

The temperature T_r is calculated by applying the 1st law on the reactor wall and on the reactants:

$$\dot{m}_{NH3} \cdot \left(\frac{\Delta h_r}{M_{NH3}} - Cp_{NH3}(T_r - T_{exh}) \right) = (UA)_r \cdot \left(T_r - \bar{T}_{htf;r} \right) \quad \text{with } \bar{T}_{htf;r} = \frac{T_{out;htf;r} + T_{in;htf;r}}{2} \qquad (8)$$

$$\dot{m}_{NH3} \cdot \left(\frac{\Delta h_r}{M_{NH3}} - Cp_{NH3}(T_r - T_{exh}) \right) = (\dot{m}Cp)_{htf;r} \cdot \left(T_{out;htf;r} - T_{in;htf;r} \right) \qquad (9)$$

Taking into account that $\frac{\Delta h_r}{M_{NH3}} >> Cp_{NH3}(T_r - T_{exh})$:

$$T_r \approx T_{in;htf;r} + \frac{\dot{m}_{NH3}.\Delta h_r}{M_{NH3}} \cdot \left(\frac{1}{2.(\dot{m}Cp)_{htf;r}} + \frac{1}{(UA)_r} \right) \qquad (10)$$

Where $T_{out;htf;r}$ and $T_{in;htf;r}$ are the outlet and inlet temperatures of the reactor heat transfer fluid; $(\dot{m}Cp)_{htf;r}$ is the heat capacity flow of the reactor HTF; $(UA)_r$ is the heat transfer parameter of the reactor.

By combining eq.3, 6, 7 and 10, the power of working fluid expansion can be expressed as:

$$\dot{W}_{NH_3} = \dot{m}_{swept} \cdot \eta_{is} \cdot Cp_{NH3} \cdot T_{adm} \cdot \left(\left(\frac{p_{adm} \cdot \left(1 - \frac{\dot{m}_{NH3}}{M_{NH_3} \cdot n_{salt} \cdot \nu_{react} \cdot \tilde{k}_{cin}} \right)}{p_{eq}(T_r)} \right)^{\frac{1-\gamma}{\gamma}} - 1 \right) \qquad (11)$$

The eq. 4, eq.10 and eq.11 show that the power of working fluid expansion $\left(\dot{W}_{NH_3}\right)$ is mainly a function of two operating parameters: the admission pressure (p_{adm}), the expander rotational speed (ω), and one design parameter which is the heat transfer parameter $(UA)_r$ of the reactor HTF. An analysis of the evolution of $\dot{W}_{NH_3}$ by varying these 3 parameters has been carried out. All other parameters are kept constant and their values represent the characteristics of the prototype (design values or values identified from the first experiments), as shown below in Table 1.

Table 1. Main design and operating parameters for the numerical coupling analysis

Expander parameter	Value	Reactor parameter	Value
Swept volume V_{swept}	1.45×10^{-5} m^3	Number of mole of salt n_{salt}	235.9 mol
Coef. of internal leakage K_{leak}	1×10^{-6} m^{3}s^{-1}.Pa$^{0.5}$	Kinetic of the reaction $\bar{k}_{cin}$	1.5×10^{-4} s^{-1}
Isentropic efficiency η_{is}	0.6	Enthalpy of the reaction Δh_r	50.59 kJ.mol^{-1}
Admission temperature T_{adm}	20 °C	HTF heat capacity flow $(\dot{m}Cp)_{htf;r}$	1000 W.K^{-1}
		HTF inlet temperature $T_{in;htf;r}$	40 °C

The increase of the expander rotation speed (ω), (Figure. **2**), induces an increase of the swept flow and thus an increase of the working fluid mass flow $\left(\dot{m}_{NH_3}\right)$, (cf. eq. 4). This increase in the mass flow rate causes a decrease of the pressure ratio (R_p) due to the increase of the reactor's temperature (T_r), (cf. eq. 10), and an increase of the pressure difference between the exhaust pressure and the equilibrium pressure of the reaction, (cf. eq. 7). These two antagonism evolutions generate an optimum of the expansion power $\left(\dot{W}_{NH_3}\right)$. For a given rotation speed, the swept mass flow rate $\left(\dot{m}_{swept}\right)$ is fixed, and thus the increase of the total mass flow rate $\left(\dot{m}_{NH_3}\right)$ with the rise of $(UA)_r$ is related to the increase in the leaked flow $\left(\dot{m}_{leak}\right)$ generated by the higher pressure ratio. While the admission pressure is fixed (p_{adm} =1.5×10^5 Pa), the enhancement of the reactor heat transfer parameter $\left((UA)_r\right)$ allows the decrease of the reactor temperature (T_r), (cf. eq. 10), and thus a decrease of the exhaust pressure (p_{exh}) resulting in a higher-pressure ratio. Thus, this higher-pressure ratio generates a rise in the power output with $(UA)_r$.

On the other hand, increasing the inlet pressure of the expander (Figure. **3**) induces an increase of the mass flow (cf. eq. 4). As for the previous analysis, this higher mass flow generates a decrease in the pressure ratio (Figure. **3** centre). In the case of low heat transfer parameter $(UA)_r$ at the reactor, these two behaviours lead to a decrease in the produced power, but for higher heat transfer parameters, an optimum of power production is detected (Figure. **3** right).

This coupling between the expander and the reactor has also been analysed experimentally, and presented in the following section. Experimentally, the rotational speed of the expander is modulated by a variable electrical resistor

which is connected to the electrical generator at the expander's extremities. The variation of the admission pressure is generated by a modification of the cold source temperature T_{cold}.

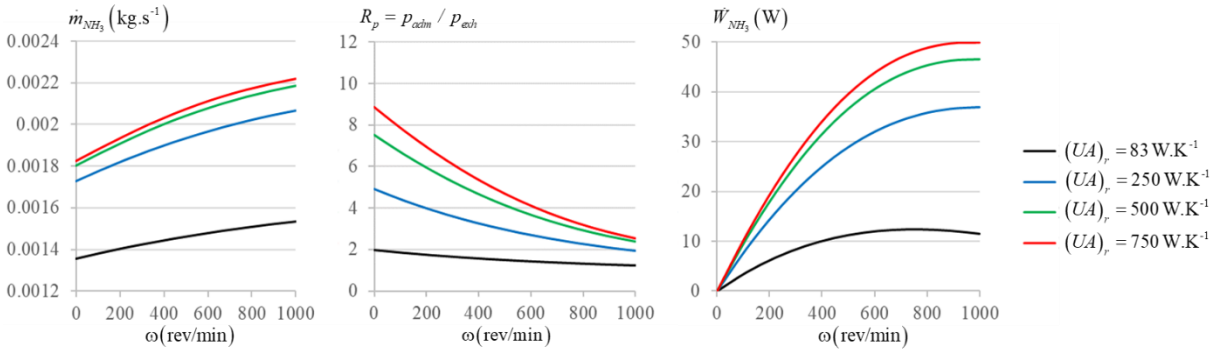

Figure. 2. Evolution of the working fluid flow rate (left), the pressure ratio (centre), the power of working fluid expansion (right) as function of the expander rotational speed for different reactor heat transfer parameter with p_{adm} =1.5×10^5 Pa.

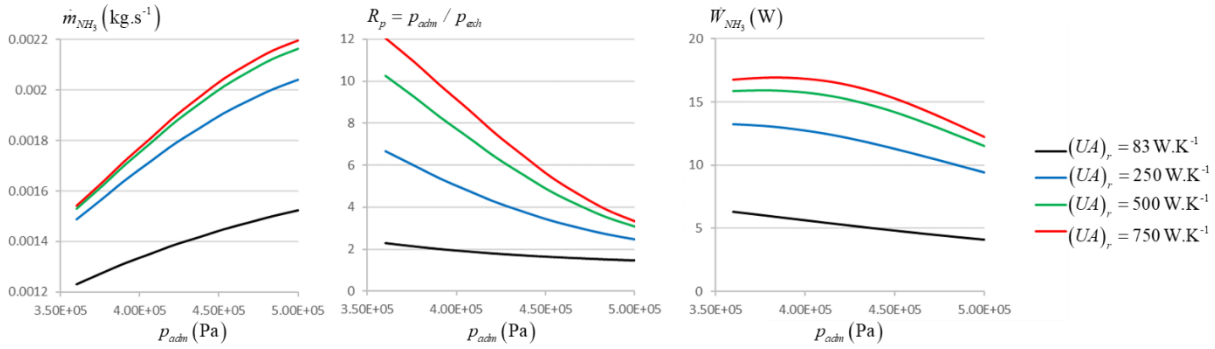

Figure. 3. Evolution of the working fluid flow rate (left), the pressure ratio (centre), the power of working fluid expansion (right) s function of the admission pressure for different reactor heat transfer parameter with ω =200 rev/min.

3. Experimental Analysis

The thermochemical cycle (reactor – condenser – evaporator) was set firstly under experimentations, by bypassing the expander. Several decomposition and synthesis reactions were done to check the reproducibility and the kinetics of the phases. Once validated [14], the expander was integrated to exploit the hybrid cycle in the discharging phase, where ammonia passes from the liquid tank to the evaporator, expander, and then to the reactor. Two protocols are set to be followed during the test of the hybrid cycle:

- The first is to fix the inlet pressure at the expander (and thus T_{cold} i.e. T^{in} and P^{in} of the expander) while varying the electrical load at the generator which will vary the coupling force with the expander, and its mechanical power. While the mechanical power is expressed as function of the pressures at the extremities of the expander, as shown in the following equation, this protocol leads to vary the outlet pressure at the expander with the electrical load and thus permits to analyse the behaviour of the cycle in such conditions.

$$\dot{W}_{mec} = \mathbf{T}_{mec}.\omega = \dot{W}_{NH_3}.\eta_{mec}$$

where $\dot{W}_{mec}$is the produced mechanical power, $\mathbf{T}_{mec}$ is the torque force between the generator and the expander, ω is the rotational speed, η_{mec} is the mechanical efficiency of the expander.

- The second is to vary the inlet pressure at the expander (and thus T_{cold}), permitting to analyse the behaviour of the expander during the discharging phase while coupled to a fixed electrical load, and thus the same coupling force with the generator.

3.1. Fixed Tcold and variable electrical charge

A first experiment with an electrical resistor of 7 Ω, connected to the generator, is done while exploiting the expander in the hybrid cycle, for a fixed T_{cold} at 10 °C at the evaporator's inlet. The inlet temperature at the reactor is set to be maintained at a medium temperature 40 °C. After the concept's validation in this experiment, more experiments are done with changing the electrical resistance to: 3.4, 31, 57, 85, 100 Ω. An experiment with a blocked expander is conducted to simulate short circuit electrical conditions, and another one without electrical charge to simulate open circuit electrical conditions, i.e. a resistor of ∞ Ω, leading to define the behaviours of the cycle at the electrical condition boundaries. In Figure. **4**, results of this first experiment are presented. The expander is rotating continuously during the whole synthesis reaction stage i.e. for a reaction advancement X between 0.1 and 0.9, proving the concept of the hybrid thermochemical cycle. After the start-up phase, the rotational speed ω of the expander decreases from 600 tr/min (i.e. the classical peak of a reaction at its beginning) till 80 tr/min for an advancement X < 0.3. Behind, an acceleration in the production is noticed where the rotational speed increased to reach 300 tr/min. Such two-level profile is also repeated in the other experiments, where the cold production and the mechanical work have always two levels during the reaction – under actual analysis. For this system analysis, results are treated as average values between the minimum and the maximum level production limits that correspond to an average of the production during an advancement of the reaction between 0.2 & 0.8.

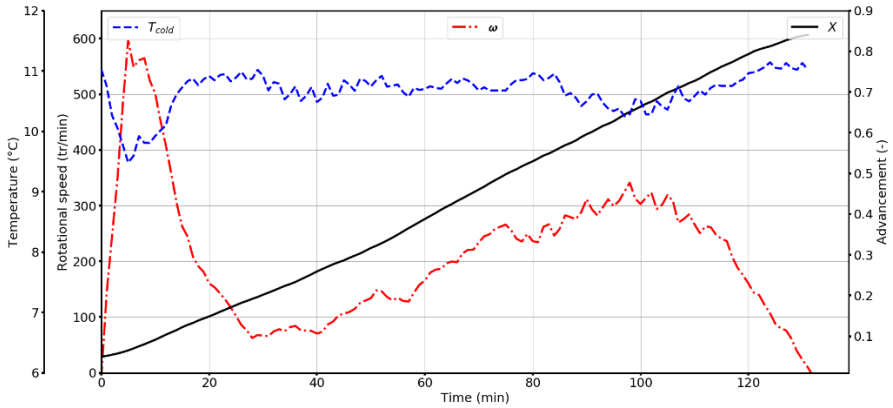

Figure. 4. Cold temperature, rotational speed of the expander during the discharging phase.

Figure. **5**, Figure. **6**, and Figure. **7** present the behaviour of the hybrid cycles for different electrical resistances. Figure. **5** presents the variation of the rotational speed ω_{av} of the expander, and the torque force $\mathbf{T}_{mec,av}$ with the generator as function of the electrical resistor. When the expander is free, or the generator is in an open circuit electrical condition, the rotational speed reaches its maximum value while the torque force has its minimum. Coupling the electrical resistor to the generator increases the torque force on the expander and decreases its rotational speed. The maximum average rotational speed achieved by the expander was at 480 tr/min in an open circuit electrical condition. Regarding the average torque force, its maximum was at 1 N.m for a blocked expander, while the minimum was at 0.1 N.m for the open circuit experiment.

Figure. **6** shows the variation of the average mass flow rate of ammonia $\dot{m}_{av}$ and the average pressure ratio $R_{p,av}$ at the expander as function of the electrical resistor. The average mass flow rate has an increasing profile as the electrical resistance increases, whereas the pressure ratio has a decreasing one. The maximum pressure ratio achieved during the experiments is for the blocked case experiment, where $R_{p,av}$ = 1.5 and the minimum is for an open circuit electrical condition experiment, $R_{p,av}$ = 1.2. Regarding the mass flow rate of ammonia, the difference between experimental boundaries (blocked and open circuit conditions) is of 0.175 g/s. On the other side, concerning the productions of the cycle, Figure. **7**, the cold production has a negligible variation between the boundaries of the experiments, but although it shows an increasing profile while the electrical resistance increases ($Q_{c,av}$ from 1.98 to 2.1 kW). This slight increase in the cold production results from the slight increase in the mass flow rate of ammonia as the conditions changes from blocked to an open circuit. No mechanical productions are achieved while the expander is blocked, an average of 6 W is produced in open circuit conditions, and a maximum of 10.5 W is reached for a resistance of 7 Ω. The mechanical production increases to reach a maximum and then decreases while the electrical load at the generator increases presenting an optimum of the mechanical production between the blocked conditions and the experiment with an electrical resistor of 31 Ω, contrary to the cold production that increases always with the electrical resistance. This cycle's behaviour, shows the antagonistic coupling behaviour between the cold production and the mechanical power as the electrical resistance varies,

determining an optimum of the mechanical power production dependent on the mass flow rate of the gas, the coupling force and the pressure ratio at the expander.

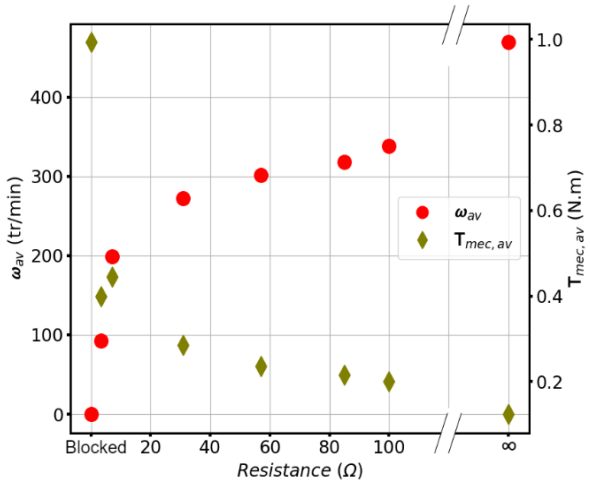

Figure. 5. Variation of the rotational speed and the mechanical torque at the expander with the electrical resistance.

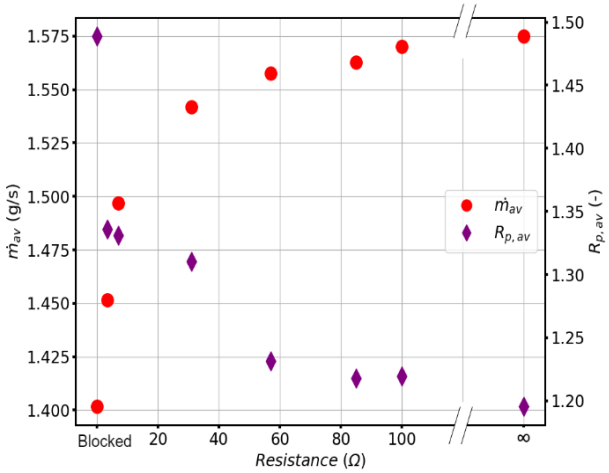

Figure. 6. Average ammonia flow rate and pressure ratio variations with the electrical resistance.

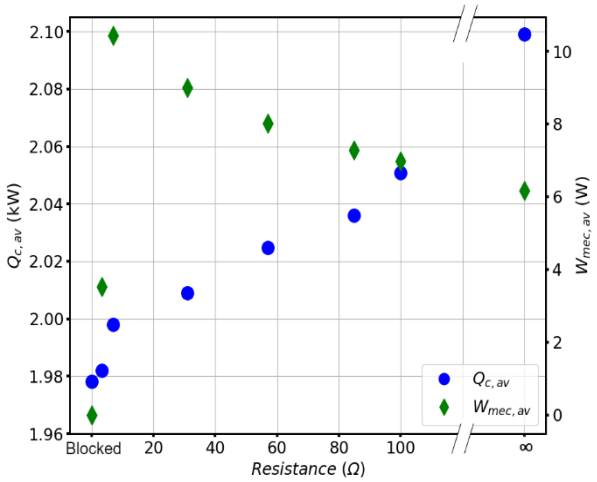

Figure. 7. Variation of the average cold and mechanical productions with the electrical resistance.

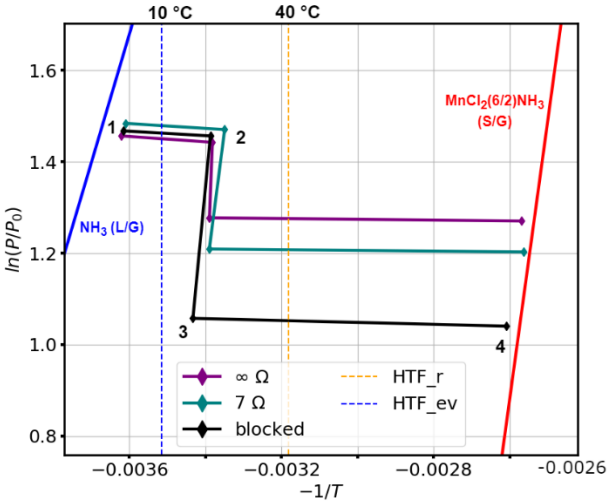

Figure. 8. Clausius Clapeyron diagram: experiments with constant Tcold but variable electrical conditions.

Whereas, the cold production is shown to be dependent on the mass flow rate as the evaporating pressure is set to be fixed by T_{cold}. These experimental results that show weak pressure ratios and mechanical productions highlight the importance of the expander's technology necessary for such hybridization objective, where such results determine an important internal leakage inside the scroll expander that affects the mechanical behaviour and the mass coupling between the components. Additionally, Figure. **5**, Figure. **6** and Figure. **7**, show that experiments done between a blocked resistor and a resistor of 31 Ω, have more important and interesting evolution of the cycle's behaviour since after this boundary its seems that the behaviour don't have a significant change - stable. Therefore, this demands to define operating electrical conditions more adaptable to the range of production of the expander in such cycles of small gas flow rates.

Within such limitation and weak productions, Clausius Clapeyron diagram in Figure. **8** still shows the mass coupling between the components of the hybrid cycle at the electrical boundary conditions and at 7 Ω (chosen since it's the cycle that achieved the maximum mechanical power). For each experiment representation on this diagram:

HTF_ev and HTF_r represents the heat transfer fluid conditions at the evaporator and the reactor respectively, points 1, 2, 3, represent respectively the temperature and pressure of ammonia at the evaporator, at the inlet of the expander, at the outlet of the expander and point 4 represents the salt's temperature and pressure during the reaction. This diagram presents clearly the difference with the classical one (where the synthesis pressure is the same as the evaporating pressure in a classical cycle but different in a hybrid one - points 1 & 4) and shows the expansion of ammonia at the expander (points 2 – 3) even with its weak ratio. Furthermore, it sheds attention to the importance of the heat sink and exchange at the reactor (to evacuate the heat of the synthesis reaction) while the salt's temperature is closer to the equilibrium temperature of the reaction than the heat transfer fluid temperature at the reactor's level.

3.2. Variable cold temperature and fixed electrical charge

Three experiments were done at three different cold temperatures: 5, 10, and 15 °C (by the glycolic water heat transfer fluid loop of the evaporator) corresponding to $P_{sat,evap}$: 5.12, 6.12, and 7.28 bar respectively. An electrical resistor of 7 Ω is connected to the generator that's coupled to the expander. The inlet temperature at the reactor is set to be maintained at a medium temperature of 40 °C (by an oil HTF loop). The following figures (Figure. **9** and Figure. **10**) present the behaviour of the hybrid cycles for these 3 cold temperatures. For a better analysis, the experimental operating conditions are plotted on the Clausius Clapeyron diagram, Figure. **11**.

The average cold production $Q_{c,av}$ at the evaporator and the average mass flow rate of ammonia $\dot{m}_{av}$ are shown in Figure. **9** and Figure. **10** for the three experiments. As T_{cold} increases (i.e. P_1 in Figure. **11**), the average mass flow rate of ammonia increases. This is due to a larger deviation from the equilibrium conditions of the synthesis reaction (i.e. the difference between T_{HTF-r} and $T_{eq}(P_3)$ in Figure. **11**). This increase in the flow rate of the gas increases the average cold power production, as expected. Despite in these experiments the minimum cold temperature is fixed at 5 °C and the maximum at 15 °C, corresponding to 2.16 bar as a pressure difference between the minimum and maximum operating conditions at the evaporator' level, the difference between the average cold productions slightly changed where the average production increases from 1.85 to 2.25 kW with the increase of the average mass flow rate from 1.4 to 1.75 g/s as the cold temperature increases. At the level of the expander, the average mechanical production $\dot{W}_{mec,av}$ and the average pressure ratio $R_{p,av}$ between the inlet and the exhaust pressures are shown in Figure. **9** and Figure. **10**. The average mechanical power decreases from 10.2 to 9.6 W and the average pressure ratio from 1.55 to 1.22, as the cold temperatures increases from 5 to 15 °C. The Clausius Clapeyron diagram Figure. **11** shows for the three experiments that the salt's temperature is mostly close to its equilibrium and far from the imposed heat transfer fluid temperature HTF_r. This increase of the temperature difference between the reactive medium and the HTF, that's proposed to be a result of the weak heat transfer parameters at the reactor, imposes a higher pressure at the expander's exhaust. In the ideal case, without heat transfer limitations at the reactor, the pressure in the reactor P_3 would be smaller for the 3 cases and thus the pressure ratio of the expander $R_p = P_{in}/P_{out} = P_2/P_3$ would increase with T_{cold}, but, the experimental results show the inverse ($R_{p,av}$ = 1.49, 1.26, 1.19 for T_{cold} = 5, 10 and 15 °C respectively).

Therefore, while T_{cold} and the evaporating pressure P_1 increases, the mass flow rate of ammonia increases, which must favour in terms the mechanical power at the expander, but while on the other hand the pressure ratio of the expander decreases, the mechanical power is reduced. This behaviour demonstrates the coupling between the reactor and the expander, and numerical studies are in progress to deeper analyse this coupling, thanks to these experimental results. Besides the effect of the hot reactive medium temperature, the decrease in the pressure ratio while the evaporating pressure increases results from an important internal leakage through the scroll expander. Therefore, the leaked flow rate which flows directly to the reactor is significantly higher than the effective mass flow rate, rising the pressure at the reactor inlet, and thus resulting in low pressure ratios and an unexpected decrease in the mechanical work. This analysis, in this protocol, highlight again the important mass coupling between the expander and the reactor, with an attention to the expander's technology and the heat exchange at the thermochemical reactor during the synthesis reaction.

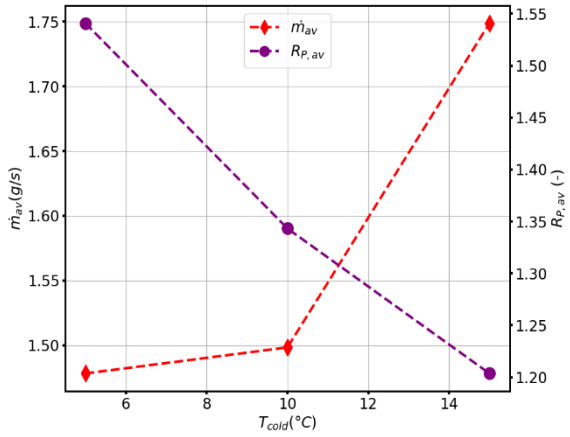

Figure. 9. Variation of the average mass flow rate and pressure report with Tcold.

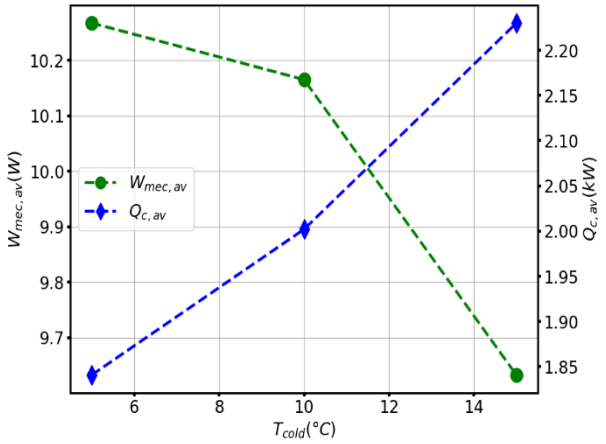

Figure. 10. Average mechanical and cold power variations with Tcold.

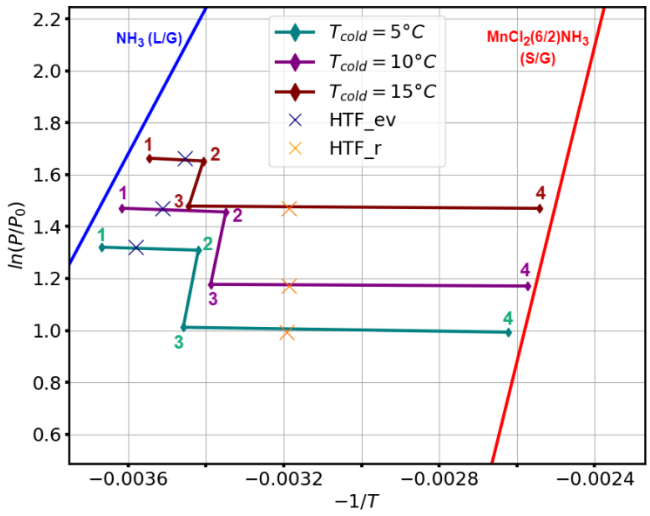

Figure. 11. Clausius Clapeyron diagram: Fixed electrical condition but variable Tcold.

4. Conclusion

A hybrid thermochemical prototype was developed at CNRS-PROMES laboratory, providing the reliability and concept validation of such hybrid cycles. Such cycle is able to recover heat at low and medium ranges below 250 °C, showing its adaptability to the integration in industrial parks for heat waste recovery. After a steady state analysis of the coupling between the expander and the reactor, first experimental tests at the laboratory showed this mass coupling behaviour between the expander and the reactor in several operating conditions. At their limits, the experiments highlight the importance of the heat sink and thermal exchanges at the reactor's level and shed attention on the technology of the expander regarding its internal leakage, as concluded from the experiments done with a fixed electrical load and variable evaporating pressures. On the other side, the experiments with a fixed evaporating pressure and variable electrical resistances defined an optimum of the mechanical production at the expander's level and showed the possibility of a control methodology at the generator's level to maintain the pressure of the synthesis reaction (or the expander's exhaust). While it could be noted that such hybrid cycle achieves the first experimental success based on what's presented in the literature, motivations to perform experimental tests on other hybrid thermochemical architectures are considered. In parallel, a numerical model developed in a previous study is set to be validated in order to go deeper in the energetic and exergetic analysis of the cycle.

Acknowledgments

This work has been financially supported by the French National Research Agency (ANR) for the purpose of the ThermHyVal project under contract ANR-20-CE05-0036 (https://anr.fr/Projet-ANR-20-CE05-0036) and by a prematuration program of the French National Centre for Scientific Research (CNRS).

Nomenclature

$CaCl_2$	calcium chloride
C_p	specific heat capacity
h	enthalpy
htf	heat transfer fluid
HTF_ev	heat transfer fluid at the evaporator
HTF_r	heat transfer fluid at the reactor
K_{leak}	leakage loss coefficient
$\bar{k}_{cin}$	kinetics of the reaction
$\dot{m}$	mass flow rate
M	molar mass, kg/mol
$MnCl_2$	Manganese (II) chloride
n	number of moles, mol
NH_3	ammonia
P	pressure, bar
Q	thermal power
R	ideal gas constant, J/(K.mol)
Rp	pressure ratio
T	temperature, °C
T	torque, N.m
UA	conductance parameter, W/K
$\dot{W}$	expansion power, W
$\dot{W}_{mec}$	mechanical power, W
X	advancement, -

Greek symbols

η	efficiency
$\boldsymbol{\omega}$	rotational speed, tr/min
ν	stoichiometric coefficient
Δ	variation
γ	adiabatic coefficient

Subscripts

av	average
cond	condensation
evap	evaporation
h	hot
cold	cold
syn	synthesis
swept	suction chambers
leak	leakage
adm	admission
exh	exhaust
is	isentropic

r	reactor
eq	equilibrium
sat	saturation
c	cold
in	inlet
out	outlet
mec	mechanical
amb	ambient

References

[1] Brundtland G, Khalid M, Agnelli S, *et al*. Our common future: the world commission on environment and development. Oxford: Oxford University Press; 1987.

[2] M.S. Choudhari, V.K. Sharma, M. Paswan, Metal hydrides for thermochemical energy storage applications, Int. J. Energy Res. 45 (2021)1–28.

[3] United Nation Environment Program. Division of technology, industry, and economics (UNEP DTIE), cleaner production (CP) activities; 2004

[4] Neveu P, Castaing J. Solid-gas chemical heat pumps: Field of application and performance of the internal heat of reaction recovery process. Heat Recover Syst CHP 1993;13(3):233–51. doi.org/10.1016/0890-4332(93)90014-M.

[5] Wang L, Ziegler F, Roskilly AP, *et al*. A resorption cycle for the cogeneration of electricity and refrigeration. Appl Energy 2013;106:56–64. doi.org/10.1016/j.apenergy.2013.01.041.

[6] Bao H, Wang Y, Roskilly AP. Modelling of a chemisorption refrigeration & power cogeneration. Appl Energy 2014;119:351–62 doi.org/10.1016/j.apenergy.2014.01.012

[7] Bao H, Wang Y *et al.* Chemisorption cooling and electric power cogeneration system driven by low grade heat. Energy 2014;72:590–8. doi.org/10.1016/j.energy.2014.05.084.

[8] Jiang L, Wang LW *et al*. Experimental study on a resorption system for power and refrigeration cogeneration. Energy 2016;97:182–90. doi.org/10.1016/j.energy.2015.12.128

[9] Jiang L, Wang LW, *et al*. Performance prediction on a resorption cogeneration cycle for power & refrigeration. Renew. Energy 2015;83. doi.org/10.1016/j.renene.2015.06.028.

[10] Godefroy A, Perier-Muzet M *et al*. Thermodynamic analyses on hybrid sorption cycles for low-grade heat storage & cogeneration of power & refrigeration. Appl Energy 2019;255:113751. doi.org/10.1016/j.apenergy.2019.113751.

[11] Godefroy A, Perier-Muzet M, Mazet N. Novel hybrid thermochemical cycles for low-grade heat storage and autothermal power generation. Appl Energy 2020;270:115111. doi.org/10.1016/j.apenergy.2020.115111.

[12] Godefroy A, Perier-Muzet M *et al*. Hybrid thermochemical cycles for low-grade heat storage & conversion. ECM 2020;225 doi.org/10.1016/j.enconman.2020.113347

[13] Godefroy A. Analyse thermodynamique et performances dynamiques de cycles hybrides impliquant des procédés sorption. PhD, U.Perpignan,2020.theses.hal.science/tel-03051549

[14] Ghazale H., Morel G., Godefroy A., *et al*. Procédé thermochimique hybride de stockage et conversion en froid et électricité d'une source thermique basse température. (SFGP 2022). sfgp2022.fr/fr/soumissions/resumes-a-telecharger.html - Transition energétique/